Smart Structures and Systems, Vol. 3, No. 4 (2007) 423-437
DOI: http://dx.doi.org/10.12989/sss.2007.3.4.423

Identification of nonlinear elastic structures using empirical mode decomposition and nonlinear normal modes

C. W. Poon† and C. C. Chang‡

Department of Civil Engineering, Hong Kong University of Science and Technology, Clear Water Bay, Kowloon, Hong Kong

(Received February 20, 2006, Accepted January 10, 2007)

Abstract. The empirical mode decomposition (EMD) method is well-known for its ability to decompose a multi-component signal into a set of intrinsic mode functions (IMFs). The method uses a sifting process in which local extrema of a signal are identified and followed by a spline fitting approximation for decomposition. This method provides an effective and robust approach for decomposing nonlinear and non-stationary signals. On the other hand, the IMF components do not automatically guarantee a well-defined physical meaning hence it is necessary to validate the IMF components carefully prior to any further processing and interpretation. In this paper, an attempt to use the EMD method to identify properties of nonlinear elastic multi-degree-of-freedom structures is explored. It is first shown that the IMF components of the displacement and velocity responses of a nonlinear elastic structure are numerically close to the nonlinear normal mode (NNM) responses obtained from two-dimensional invariant manifolds. The IMF components can then be used in the context of the NNM method to estimate the properties of the nonlinear elastic structure. A two-degree-of-freedom shear-beam building model is used as an example to illustrate the proposed technique. Numerical results show that combining the EMD and the NNM method provides a possible means for obtaining nonlinear properties in a structure.

Keywords: empirical mode decomposition; nonlinear normal mode; nonlinear identification.

1. Introduction

Fourier transform (FT) has been used commonly for extracting structural dynamic characteristics from measured vibration responses. Despite its simplicity and long history of application, the FT suffers from a few shortcomings. The FT decomposes a time-domain signal into a superposition of constant-frequency trigonometric functions. As commented by Huang, *et al*. (1998a), the Fourier spectral analysis is restricted to linear systems and the signal to be processed should be either periodic or stationary. The FT is not able to reveal the time dependency of a signal and fails to capture the evolutionary characteristics that commonly observed in the signal measured from naturally-excited structures (Gurley and Kareem 1999). As the Fourier spectrum defines harmonic components globally, additional harmonic components are needed to simulate non-stationary data or data that contain

†PhD Candidate, E-mail: cecwpoon@ust.hk
‡Associate Professor, E-mail: cechang@ust.hk

nonlinear effects. This eventually leads to spurious harmonic components and causes misleading energy-frequency distribution (Huang, *et al*. 1998a). Wavelet transform (WT) may be viewed as an extension of the FT with adjustable window location and size. It allows an arbitrary function to be expressed as a series expansion where each term is one of the local basis wavelets multiplied by its magnitude. This use of local wavelet functions provides the WT with a flexibility to allow for simultaneous time-frequency resolution for non-stationary data. Another approach that shows a potential for time-frequency decomposition of non-stationary and/or nonlinear data is the Hilbert transform (HT). Feldman (1994a, b) developed a HT based method to identify instantaneous modal parameters of nonlinear single-degree-of-freedom (SDOF) systems under free and forced vibration. In this method, the HT is first applied on the free decay response of a nonlinear SDOF system to form an analytic signal. The nonlinear damping and stiffness of the systems can then be determined from the time-dependent phase angle and amplitude of the analytic signal. As the HT is applicable to signals containing only one major component, Huang, *et al*. (1998a, b) proposed an empirical mode decomposition (EMD) method prior to the use of HT. This EMD method can decompose a signal into a superposition of intrinsic mode functions (IMFs) that contain one major mode at any time instant. Since the decomposition is based on the local time-scale characteristic of data, it is applicable to non-stationary and nonlinear data. This innovative combination of EMD and HT, also known as the Hilbert-Huang transform (HHT), has shown a great potential in almost all disciplines that require analyzing non-stationary and nonlinear time history data. For civil engineering applications, Yang, *et al*. (2003a, b) proposed a HHT based method to identify the normal modes and the complex modes of multi-degree-of-freedom (MDOF) linear systems using free vibration responses. Their results demonstrated that the method can be used for damage identification and health monitoring of structures. Nevertheless, like most of the other vibration-based techniques, these results are obtained assuming that the structures under monitoring exhibit linear behavior both before and after damage. Farrar, *et al*. (2001) stated that a predominantly linear structure could exhibit some degrees of nonlinearity when it was damaged. One such example is the damage involving cracks that open and close when the structure is subjected to external loads. Hence it is necessary to develop applicable algorithms that can be used to monitor or characterize nonlinear behavior in structures for the purpose of either damage identification or health monitoring of these structures. As reviewed above, the EMD method provides an effective and robust approach for decomposing nonlinear and non-stationary signals. The IMF components however do not automatically guarantee a well-defined physical meaning. Hence it is necessary to validate the IMF components carefully prior to any further processing and interpretation. In this paper, an attempt to use the EMD method to identify properties of nonlinear elastic multi-degree-of-freedom structures is explored. It is first shown that the IMF components of the displacement and velocity responses of a nonlinear elastic structure are numerically close to the nonlinear normal mode (NNM) responses obtained from two-dimensional invariant manifolds. The IMF components can then be used in the context of the NNM method to estimate the properties of the nonlinear elastic structure. A two-degree-of-freedom shear-beam building model is used as an example to illustrate the proposed technique.

2. Hilbert-Huang transform (HHT)

Huang, *et al*. (1998a) proposed the EMD method to decompose a multi-component signal $s(t)$ into a set of mono-component signals known as the IMFs. This EMD method can be briefly summarized as follows:

1. Identify all extrema of $s(t)$
2. Interpolate between the minima by a cubic spline to form the envelope $e_{\min}(t)$, similarly for the maxima $e_{\max}(t)$
3. Compute the mean $\mu_1(t) = (e_{\min}(t) + e_{\max}(t))/2$
4. Subtract the mean from the signal $h_1(t) = s(t) - \mu_1(t)$

The above procedure is known as the sifting process. Since the spline fitting involves approximation, the sifting process has to be iterated. In the second sifting process, $s(t)$ is replaced by $h_1(t)$ in step 1 and step 4 becomes $h_{11}(t) = h_1(t) - \mu_{11}(t)$. The process is iterated k times until $h_{1k}(t) = h_{1(k-1)}(t) - \mu_{1k}(t)$ satisfies two conditions: (1) $h_{1k}(t)$ is a mono-component, i.e., the difference between the number of zero crossing (including up-crossing and down-crossing) and number of extrema is at most one; and (2) $h_{1k}(t)$ satisfies the criteria proposed by Rilling, *et al.* (2003). The criteria ensure small fluctuations in the mean globally and allow for large excursions locally. The time function h_{1k} is defined as the first IMF from the original data and designated as g_1. It contains the highest frequency component of the data. The residue r_1 is obtained by subtracting $s(t)$ by g_1. Since this residue may contain lower frequency components, it is treated as a new signal and subjected to the same sifting process as described above. This procedure can be repeated until the residue is a mean trend of the original signal. Since each IMF contains only one major component at any time instant, the HT can be applied on these IMFs individually. Given an arbitrary narrow-band time signal $g(t)$, its HT $g_H(t)$ is defined as (Hahn 1996).

$$g_H(t) = \frac{1}{\pi} P \int_{-\infty}^{\infty} \frac{g(t')}{t - t'} dt \tag{1}$$

where P is the Cauchy principal value. The functions $g(t)$ and $g_H(t)$ can be combined to form an analytic complex signal $G(t)$ as follows:

$$G(t) = g(t) + i g_H(t) = a(t) e^{i\theta(t)} \tag{2}$$

in which $a(t)$ and $\theta(t)$ are the amplitude and the phase angle of the signal and are given respectively by

$$a(t) = [g^2(t) + g_H^2(t)]^{1/2} \tag{3}$$

$$\theta(t) = \tan^{-1}\left(\frac{g_H(t)}{g(t)}\right) \tag{4}$$

Note that $\theta(t)$ is normally a fast varying time function as compared with $a(t)$. The instantaneous frequency of the analytic signal is defined as

$$\omega(t) = \frac{d\theta(t)}{dt} \tag{5}$$

3. Nonlinear normal mode (NNM)

For a nonlinear elastic structure with N degrees of freedom, the equations of motion under free vibration are given as

$$\mathbf{M}\ddot{\mathbf{x}} + \mathbf{C}\dot{\mathbf{x}} + (\mathbf{K}_0 + \mathbf{K}_n(\mathbf{x};\dot{\mathbf{x}}))\mathbf{x} = \mathbf{0} \tag{6}$$

where $\mathbf{x} = [x, x_2, ..., x_N]^{\mathbf{T}}$ is the displacement vector, and $\mathbf{M}$, $\mathbf{C}$, and $\mathbf{K_0}$ are the mass, damping and linear stiffness matrices, respectively; $\mathbf{K_n}$ represents a nonlinear stiffness matrix that can be a general function of $\mathbf{x}$ and $\dot{\mathbf{x}}$. The state-space form of Eq. (6) can be written as

$$\dot{\mathbf{z}} = \mathbf{D}(\mathbf{z})\mathbf{z} \tag{7a}$$

$$\mathbf{z} = \begin{Bmatrix} \mathbf{x} \\ \dot{\mathbf{x}} \end{Bmatrix}, \quad \mathbf{D}(\mathbf{z}) = \begin{bmatrix} \mathbf{0} & \mathbf{I} \\ -\mathbf{M}^{-1}(\mathbf{K}_0 + \mathbf{K}_\mathbf{n}) & -\mathbf{M}^{-1}\mathbf{C} \end{bmatrix} \tag{7b,c}$$

where $\mathbf{z}$ and $\mathbf{D}$ are the state vector and the nonlinear state matrix, respectively. Alternatively, Eq. (6) can also be rewritten as

$$\dot{x}_i = y_i, \quad \dot{y}_i = f_i(\mathbf{x};\mathbf{y}) \qquad i = 1,2, ..., N \tag{8}$$

Shaw and Pierre (1993) assumed that there exists at least one motion for which all displacements and velocities can be functionally related to a single displacement–velocity pair, say x_1 and y_1. For brevity, let $x_1 = u$ and $y_1 = v$, and express the other x_i's and y_i's in terms of u and v as follows:

$$x_i = X_i(u, v), \quad y = Y_i(u, v) \qquad i = 1, 2, ..., N \tag{9a,b}$$

Mathematically, Eqs. (9) describe a constraint surface of dimension two (u, v) in the $2N$-dimensional phase space. A normal mode of motion for the nonlinear elastic system can be defined as a motion that takes place on a two-dimensional invariant manifold in the system's phase space. An approximate solution for the normal mode invariant manifold near the equilibrium point has been proposed by Shaw and Pierre (1993). Eqs. (9) are first approximated by a third-order Taylor series expansion,

$$x_i \approx \alpha_{1i}u + \alpha_{2i}v + \alpha_{3i}u^2 + \alpha_{4i}uv + \alpha_{5i}v^2 + \alpha_{6i}u^3 + \alpha_{7i}u^2v + \alpha_{8i}uv^2 + \alpha_{9i}v^3 \tag{10a}$$

$$y_i \approx \beta_{1i}u + \beta_{2i}v + \beta_{3i}u^2 + \beta_{4i}uv + \beta_{5i}v^2 + \beta_{6i}u^3 + \beta_{7i}u^2v + \beta_{8i}uv^2 + \beta_{9i}v^3 \qquad i = 1,2,...,N \tag{10b}$$

where α_{ij} and β_{ij} are the Taylor series coefficients. Provided that the structural properties are given, N sets of α_{ij} and β_{ij} can be obtained by substituting Eqs. (10) into (7a) with the elimination of the time derivative terms using Eq. (8). Each of these sets correspond to a pair of (u, v) which is termed as the modal coordinates. Hence the state vector $\mathbf{z}$ in the physical domain can be related to the modal coordinate vector $\mathbf{w}$ as,

$$\mathbf{z} \approx \mathbf{\Phi}(\mathbf{w}) \cdot \mathbf{w} \tag{11}$$

$$\mathbf{\Phi}(\mathbf{w}) = \mathbf{\Phi_0} + \mathbf{\Phi_1}(\mathbf{w}) + \mathbf{\Phi_2}(\mathbf{w}) \tag{12}$$

where $\mathbf{\Phi}$ is the nonlinear mode shape matrix which is a function of $\mathbf{w}$ and the Taylor series coefficients; and $\mathbf{\Phi_0}$, $\mathbf{\Phi_1}$ and $\mathbf{\Phi_2}$ are the 0^{th}, 1^{st} and 2^{nd} order mode shape component matrices which are functions of the 0^{th}, 1^{st} and 2^{nd} order of $\mathbf{w}$, respectively. The modal coordinate vector $\mathbf{w} = [u_1, v_1,...,u_N, v_N]^{\mathbf{T}}$ consists of N modal coordinates (u_k, v_k), $k = 1, 2,..., N$. Substituting (11) into (7a) gives,

$$\left[\frac{\partial(\mathbf{\Phi w})}{\partial \mathbf{w}}\right]\dot{\mathbf{w}} = \mathbf{D} \cdot \mathbf{\Phi} \cdot \mathbf{w} \tag{13}$$

which is an explicit function of modal coordinate vector **w** only. When the structural properties are given, the time histories of **w** can be obtained from this equation.

4. EMD-NNM based characteristics identification

Assume that the state vector **z** of the nonlinear elastic structure is available from measurement. A pair of displacement and velocity time history data, let's say x_1 and $\dot{x}_1$, is selected as a reference and processed through the EMD to produce $2n$ IMF components. The selection of the data pair is rather arbitrary, except that these data must contain response from all modes. It is postulated that the obtained $2n$ IMF components can be used to form the modal coordinate vector **w**. As commented by Huang *et al.* (1998a), the IMF components do not guarantee a well-defined physical meaning just like the other decomposition methods with *a priori* basis. Hence the equivalence between the IMF components and the modal coordinate vector needs to be carefully validated in the numerical study.

Theoretically speaking, the nonlinear mode shape matrix $\mathbf{\Phi}$, in the summation form of $\mathbf{\Phi_0}$, $\mathbf{\Phi_1}$ and $\mathbf{\Phi_2}$, can be obtained using Eq. (11) via a constrained nonlinear optimization technique under given **z** and **w**. However, as suggested by Zhao ad DeWolf (1999), mode shapes of a lightly-damped system are generally insensitive to small nonlinearity. Hence, the estimation of nonlinear mode shape components $\mathbf{\Phi_1}$ and $\mathbf{\Phi_2}$ might lead to significant errors. It is suggested to approximate the nonlinear mode shape matrix using the linear mode shape matrix. Eq. (11) then becomes,

$$\mathbf{z} \approx \mathbf{\Phi}_0 \cdot \mathbf{w} \tag{14}$$

This linear mode shape matrix can be obtained from the least square fit of ratios between the IMF components at a measurement location and that at the reference location. Under this condition, Eq. (13) can be written as

$$\mathbf{\Phi}_0 \dot{\mathbf{w}} \approx \mathbf{D} \cdot \mathbf{\Phi}_0 \cdot \mathbf{w} \tag{15}$$

The nonlinear state matrix **D** that contains the physical properties of the nonlinear structure can be estimated through a constrained nonlinear optimization technique such as the sequential quadratic programming algorithm (Schittowski 1985). When the mass matrix **M** and the form of nonlinear stiffness are available, the damping matrix C and the coefficients of linear and nonlinear stiffness matrices, $\mathbf{K_0}$ and $\mathbf{K_n}$, can be obtained via Eq. (7c).

5. Illustrative examples

A 2-story shear beam building model (Fig. 1) with nonlinear stiffness is used to illustrate the applicability and accuracy of the EMD-NNM based nonlinear characteristic identification. The equations of motion for this model under free vibration condition can be written as,

$$\begin{bmatrix} m_1 & 0 \\ 0 & m_2 \end{bmatrix} \begin{Bmatrix} \ddot{x}_1 \\ \ddot{x}_2 \end{Bmatrix} + \begin{bmatrix} c_{11} & c_{12} \\ c_{21} & c_{22} \end{bmatrix} \begin{Bmatrix} \dot{x}_1 \\ \dot{x}_2 \end{Bmatrix} + \begin{bmatrix} k_1 + k_2 & -k_2 \\ -k_2 & k_2 \end{bmatrix} \begin{Bmatrix} x_1 \\ x_2 \end{Bmatrix} + \begin{Bmatrix} k_{1r} x_1^3 + k_{2r}(x_1 - x_2)^3 \\ -k_{2r}(x_1 - x_2)^3 \end{Bmatrix} = \begin{Bmatrix} 0 \\ 0 \end{Bmatrix} \tag{16}$$

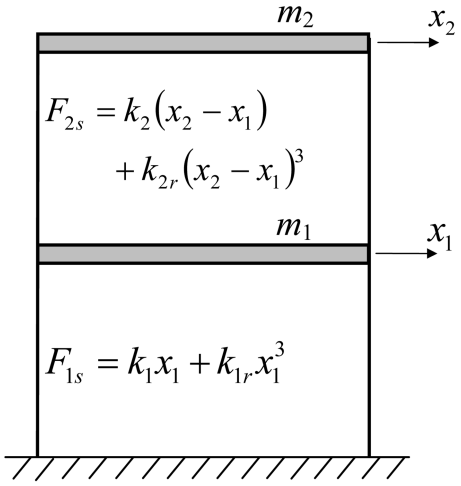

Fig. 1 Nonlinear 2-DOF shear-beam building model

The nonlinear state matrix **D** is expressed as,

$$\mathbf{D} = \begin{bmatrix} 0 & 0 & 1 & 0 \\ 0 & 0 & 0 & 1 \\ -(k_1 + k_2)/m_1 - [(k_{1r} + k_{2r})x_1^2 + 3k_{2r}x_2^2]/m_1 & k_2/m_1 + k_{2r}(3x_1^2 + x_2^2)/m_1 & -c_{11}/m_1 & -c_{12}/m_1 \\ k_2/m_2 + k_{2r}(x_1^2 + 3x_2^2)/m_2 & -k_2/m_2 - k_{2r}(3x_1^2 + x_2^2)/m_2 & -c_{21}/m_2 & -c_{22}/m_2 \end{bmatrix} \quad (17)$$

The mass and the linear stiffness coefficients for the two stories were assumed to be identical: $m_1 = m_2 = 1000$ kg and $k_1 = k_2 = 980$ kN/m, respectively. The stiffness nonlinearity was assumed to be in a cubic order with coefficients of k_{1r} and k_{2r} for the first and the second stories, respectively. Three cases were considered in this study: Case 1: linear model with $k_{1r} = k_{2r} = 0$; Case 2: nonlinearity occurs between the ground and the 1st story with $k_{1r} = -200$ MN/m^3 and $k_{2r} = 0$; and Case 3: nonlinearity occurs at both stories with $k_{1r} = k_{2r} = -200$ MN/m^3. The damping coefficients for all three cases were assumed to be the same with $c_{11} = 840$ N·s/m, $c_{22} = 560$ Ns/m, and $c_{12} = c_{21} = -280$ N·s/m. This set of damping coefficients gives a modal damping ratio of 1% for both modes of the linear model. The objective of these three case studies was to estimate the structural properties, including the damping coefficients, linear and nonlinear stiffness coefficients, assuming that the displacement and the velocity responses of the two stories were available. These responses were obtained using the Runge-Kutta (RK) method. Throughout the analysis, the two story masses were assumed to be known. The model was under free vibration with an initial condition of $x_1(0) = 0.03$ cm, $\dot{x}_1(0) = x_2(0) = \dot{x}_2(0) = 0$ for all three cases.

5.1. Case 1: Linear model

To examine the accuracy of the NNM method, the response time histories of the model was calculated via the superposition of two modal responses obtained from Eqs. (11) and (13). Fig. 2 shows the comparison of displacement and velocity responses obtained from the RK and the NNM methods. It

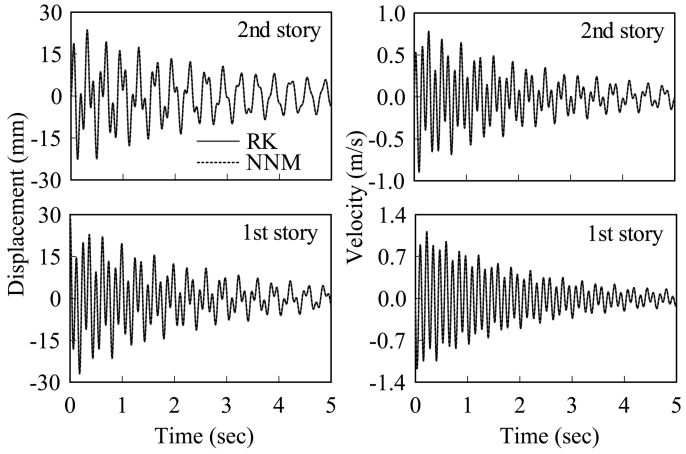

Fig. 2 Displacement and velocity responses obtained from the Runge-Kutta (RK) method and the nonlinear normal mode (NNM) method for Case 1

is seen that the responses obtained from the NNM method match perfectly with those obtained from the RK method. Next, the displacement responses at the 1st and the 2nd stories obtained from the RK method were processed through the EMD individually which resulted in two IMF components for each

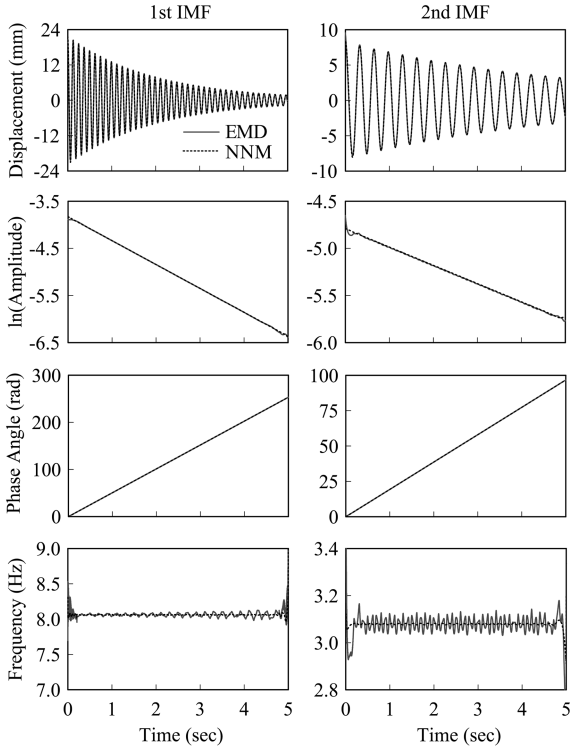

Fig. 3 Comparison of the results obtained from the IMF components of the displacement response and the NNM method for Case 1 (1st story)

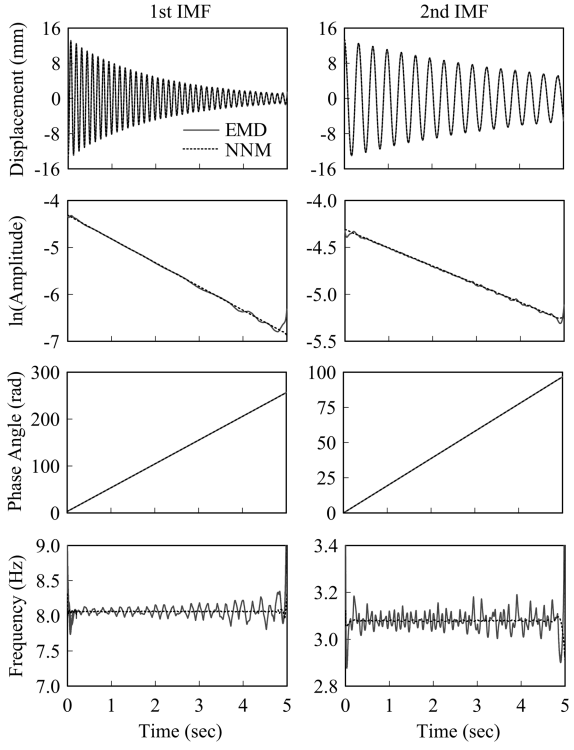

Fig. 4 Comparison of the results obtained from the IMF components of the displacement response and the NNM method for Case 1 (2nd story)

of the displacement responses. The comparison between these two IMF components and the two modal responses from the NNM method for the 1st and 2nd stories are shown in Figs. 3 and 4, respectively. It is seen that the IMF components match with the NNM responses very well. The IMF components and the NNM responses were then processed through the HT (Eq. (1)). Their amplitudes, phase angles and instantaneous frequencies were found and plotted in Figs. 3 and 4. It is seen that the phase angles obtained from the two approaches match quite well. Similarly, the amplitudes also compare quite well for the two approaches, except at the two end zones where the EMD appears to suffer from some end effects. Finally, the instantaneous frequencies obtained from the Hilbert transform of the NNM responses are pretty much constant and coincide with the analytical values of 3.08 Hz and 8.06 Hz, respectively. Those of the IMF components however fluctuate around the respective analytical values. The fluctuation might be attributed to the residual errors associated with the sifting process as commented by Rilling, *et al*. (2003). The two linear mode shapes can be obtained by comparing the corresponding IMF components of the displacement responses at the two stories as shown in Fig. 5. It is seen that the two mode shape ratios obtained from the IMF components are very close to the respective analytical values except at the two end regions. Assuming the nonlinear state matrix **D** in the form of Eq. (17), the damping coefficients and the linear and the nonlinear stiffness coefficients can be obtained from Eq. (15) using the sequential quadratic programming algorithm. The identified results are shown in Table 1. It is seen that the identified parameters are in good agreement with the assumed

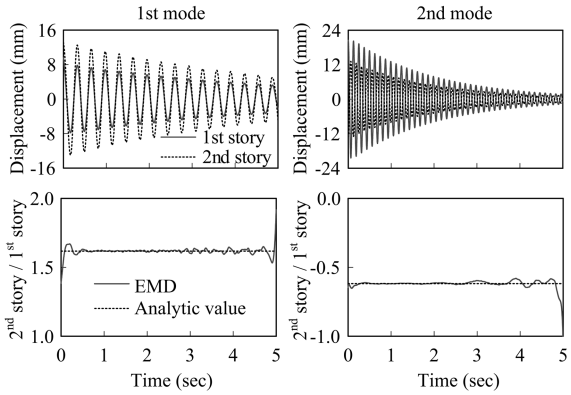

Fig. 5 IMF components obtained from the displacement responses of two stories and their amplitude ratios for Case 1

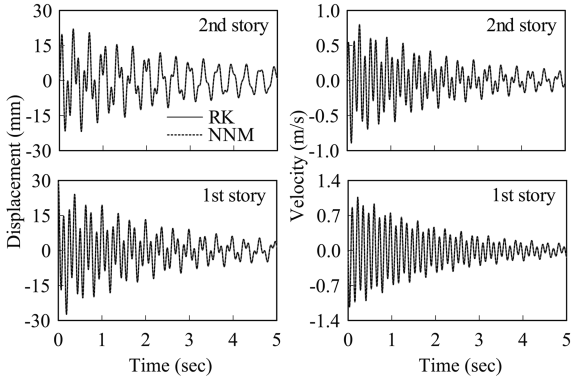

Fig. 6 Displacement and velocity responses obtained from the RK method and the NNM method for Case 2

Table 1 Parametric identification for the 2-story building model (Case 1: linear model; Case 2: nonlinearity occurs between the ground and the 1st floor; and Case 3: nonlinearity occurs at both stories)

	Property	k_1 (kN/m)	k_2 (kN/m)	c_{11} (N·s/m)	c_{12} (N·s/m)	c_{22} (N·s/m)	k_{1r} (MN/m^3)	k_{2r} (MN/m^3)
Case 1	Theoretical	980	980	840	–280	560	0	0
	Identified	973	980	817	–280	547	9	–0.5
	% error	–0.7	0.0	–2.7	0.0	–2.3	–	–
Case 2	Theoretical	980	980	840	–280	560	–200	0
	Identified	1000	968	796	–301	526	–182	0.5
	% error	2.0	–1.2	–5.2	7.5	–6.1	–9.0	–
Case 3	Theoretical	980	980	840	–280	560	–200	–200
	Identified	965	979	823	–289	559	–216	–172
	% error	–1.5	–0.1	–2.0	3.2	–0.2	8.0	–14.0

values. The errors for the linear stiffness coefficients are less than 1% and that for the damping coefficients are between 2-3%.

5.2. Case 2: Nonlinearity occurs between the ground and the 1st story

Assuming that elastic nonlinearity occurs between the ground and the 1st floor, Fig. 6 shows the comparison of displacement and velocity responses obtained from the RK and the NNM methods. It is seen that the responses obtained from the NNM method match perfectly with those obtained from the RK method for this nonlinear case. The responses from the RK method were processed through the EMD to produce IMF components. Fig. 7 shows the comparison of the IMF components and the NNM responses together with their amplitudes and phase angles for the 1st story displacement responses. It is seen that all three quantities compare quite well. After the Hilbert transform, the instantaneous frequencies from the IMF components and the NNM responses were obtained and plotted at the bottom of Fig. 7. The results show that the instantaneous frequency of the 1st IMF, corresponding to the higher mode, follows a slightly increasing trend around 8 Hz with some small fluctuations. The matching between the IMF and the NNM frequencies is excellent. As for that of the 2nd IMF, the instantaneous frequency increases from around 2.9 Hz to around 3.1 Hz as response amplitude reduces. The result from the NNM also shows a similar trend and good matching between the two results is again observed except at the end regions. These results again demonstrate that the IMF components obtained from the EMD are

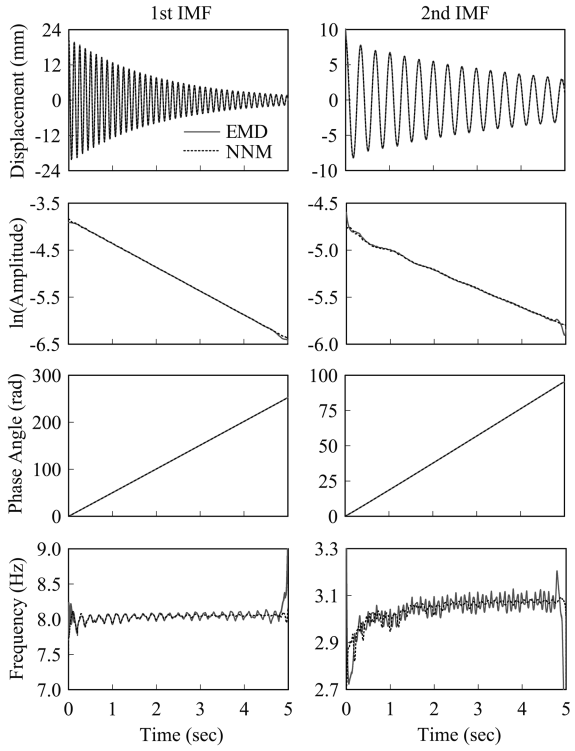

Fig. 7 Comparison of the results obtained from the IMF components of the displacement response and the NNM method for Case 2 (1st story)

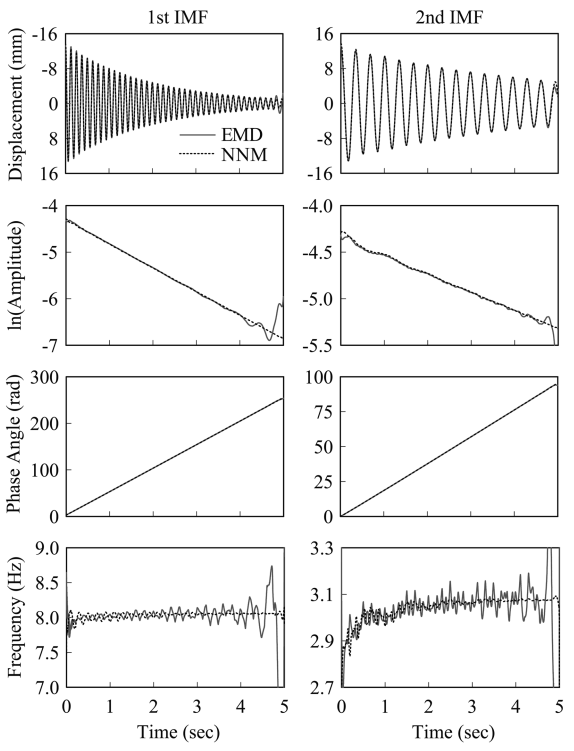

Fig. 8 Comparison of the results obtained from the IMF components of the displacement response and the NNM method for Case 2 (2nd story)

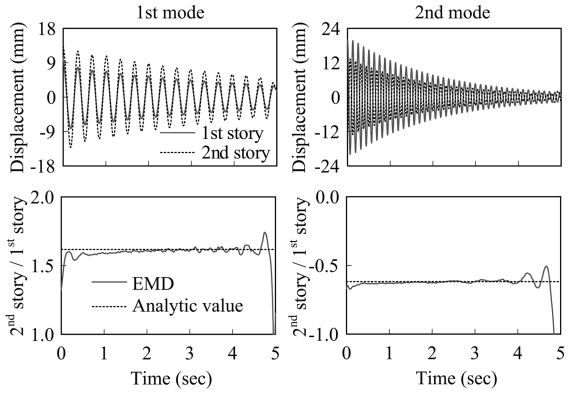

Fig. 9 IMF components obtained from the displacement responses of two stories and their amplitude ratios for Case 2

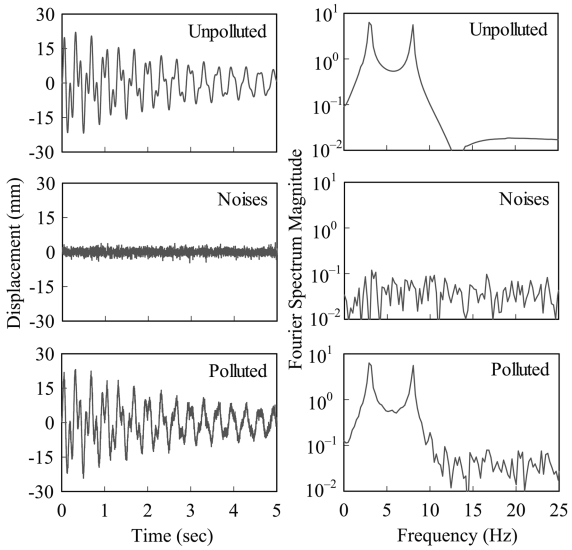

Fig. 10 Unpolluted and noise-polluted displacement responses and noises at the 2nd story for Case 2

very close to the NNM responses. Similar results and comparisons for the 2nd story are shown in Fig. 8. The two instantaneous mode shapes can be obtained by comparing the corresponding IMF components of the displacement responses at the two stories as shown in Fig. 9. It is seen that the two instantaneous mode shape ratios obtained from the IMF components are very close to the respective analytical linear mode shape values. These results confirm that the approximation of nonlinear mode shapes by linear ones as adopted by Eq. (14) is reasonable. Hence the nonlinear state matrix **D** can be obtained from Eq. (15) through the sequential quadratic programming algorithm. The identified parameters for this case are again summarized in Table 1. It is seen the errors for the linear stiffness coefficients are less than 2% and that for the damping coefficients are between 5-8%. Also note that the nonlinear stiffness coefficient k_{1r} is identified with 9% error and the value of the other nonlinear stiffness coefficient k_{2r} is quite small. This suggests that the current approach can correctly locate the occurrence of stiffness nonlinearity in the model.

In practical applications, measurement noises are almost unavoidable. It is necessary to study whether these measurement noises would affect the accuracy of the proposed technique. Assume that the measured displacement and velocity responses are polluted by measurement noises and can be expressed as follows:

$$\tilde{\mathbf{z}}(t) + \mathbf{z}(t) = \mathbf{n}(t) \tag{18}$$

The noise vector $\mathbf{n}(t) = [n_1(t)\ n_2(t) \cdots n_{2N}(t)]^{\mathrm{T}}$ consists of $2N$ independent zero-mean band-limited Gaussian white noises $n_i(t)$. The intensity of noise is described by the ratio between the root mean square of the noise and the maximum amplitude of the corresponding response (Yang, *et al.* 2003a,b). In the following analysis, noises with an intensity of 5% were assumed in the measured displacement and velocity responses. Fig. 10 shows the unpolluted and the noise-polluted 2nd story displacement

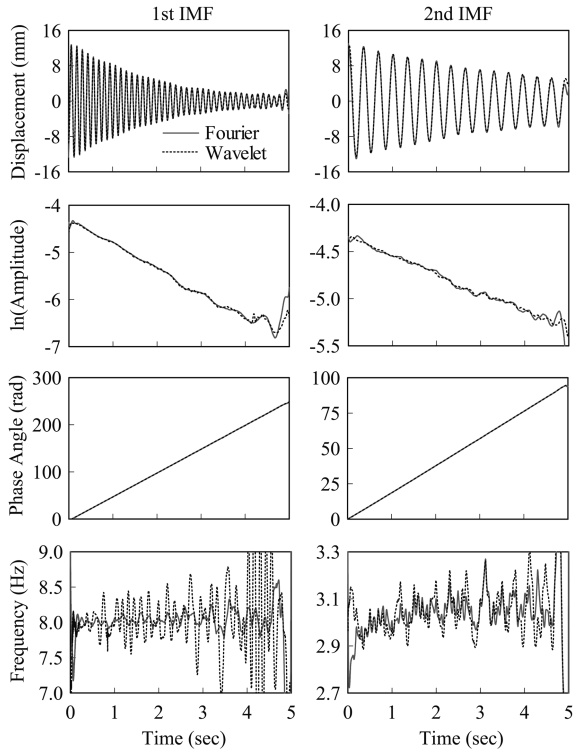

Fig. 11 Comparison of the IMF components of the displacement response for Case 2 in the presence of measurement noises (2nd story)

responses as well as their Fourier spectra. Prior to decomposing the responses through the EMD method, it was necessary to remove noises from the responses. In this study, two approaches were used for noise removal: the Fourier-based band-pass filtering technique and the wavelet-based denoising technique. The Fourier-based band-pass filtering technique for the EMD was proposed by Yang, *et a*l. (2003a), in which the measured responses were band-pass filtered with frequency bands of 25 Hz and 5-8 Hz respectively before processed through the EMD for the IMF components. The wavelet-based denoising procedure involved the following steps: (i) apply wavelet transform to the noisy signal to produce the noisy wavelet coefficients; (ii) select appropriate thresholds for each level to remove noises; and (iii) inverse wavelet transform of the thresholded wavelet coefficients to obtain a denoised signal (Donoho 1995). For this example, the Daubechies wavelet db5 was used and the decomposition was performed up to the 4^{th} level before applying a constant threshold. The wavelet filtered responses were then processed through the EMD for the IMF components. Fig. 11 shows the comparison of the two sets of IMF components for the noise-polluted 2^{nd} story displacement response processed through the Fourier-based band-pass filtering technique and the wavelet-based denoising technique, respectively. Also shown in the same figure are their amplitudes, phase angles and instantaneous frequencies. It is seen that the amplitudes and phase angles obtained from the two filtering techniques are almost indistinguishable from each other. The instantaneous frequencies however show some differences. Those obtained from the Fourier-based band-pass filtering technique appear to be less fluctuating than that from the wavelet-based denoising technique. The proposed technique was then applied on the IMF components to identify the properties of the building model. The identified results are listed in Table 2.

Table 2 Parametric identification for the Case 2 building model in the presence of 5% measurement noise

Property		k_1 (kN/m)	k_2 (kN/m)	c_{11} (N·s/m)	c_{12} (N·s/m)	c_{22} (N·s/m)	k_{1r} (MN/m^3)	k_{2r} (MN/m^3)
Fourier-based	Theoretical	980	980	840	–280	560	–200	0
	Identified	970	972	890	–284	606	–19	–7
	% error	–1.0	–0.8	6.0	1.4	8.2	–91	–
Wavelet-based	Theoretical	980	980	840	–280	560	–200	0
	Identified	970	972	897	–285	613	–175	39
	% error	–1.0	–0.8	6.8	1.8	9.5	–12.5	–

It is seen that the identified linear stiffness and damping coefficients from the two filtering techniques are not significantly affected by the presence of noise and are in good agreement with the assumed values with less than 10% differences. These findings agree with those obtained from Yang, *et al.* (2003a,b), who investigated the effect of noise for the identification of linear MDOF structures. For the nonlinear properties, the Fourier-based band-pass filtering technique however results in a 91% error for the nonlinear stiffness coefficient k_{1r}. Huang, *et al.* (1998a) commented that additional intrawave harmonic components in the Fourier analysis were needed to simulate nonlinear characteristics in a signal. As these harmonic components were removed globally by the Fourier-based band-pass filtering, hence the nonlinear properties of the structure could not be correctly identified. On the other hand, the wavelet-based denoising technique identifies the nonlinear stiffness coefficient k_{1r} to be –175 MN/m^3 which corresponds to about 12% error. The wavelet-based technique has a capability to decompose a signal in the frequency and the temporal domains simultaneously, hence the response could be denoised without significantly affecting its nonlinear characteristics.

5.3. Case 3: Nonlinearity occurs at both stories

Assuming that elastic nonlinearity occurs at both stories, Fig. 12 shows the comparison of displacement and velocity responses obtained from the RK and the NNM methods. Again, the responses obtained from the NNM method match perfectly with those obtained from the RK method

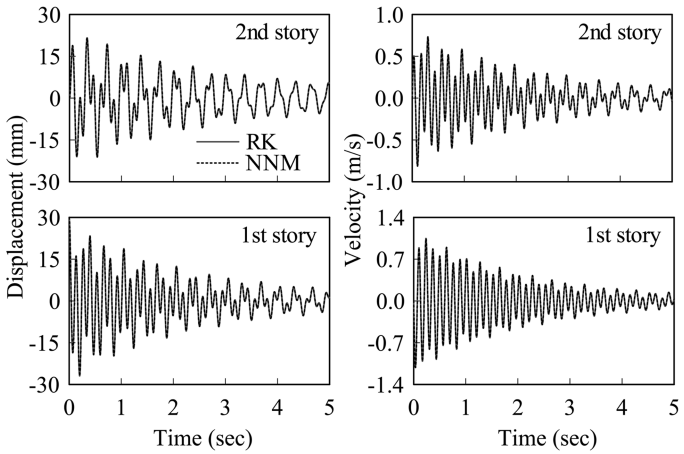

Fig. 12 Displacement and velocity responses obtained from the RK method and the NNM method for Case 3

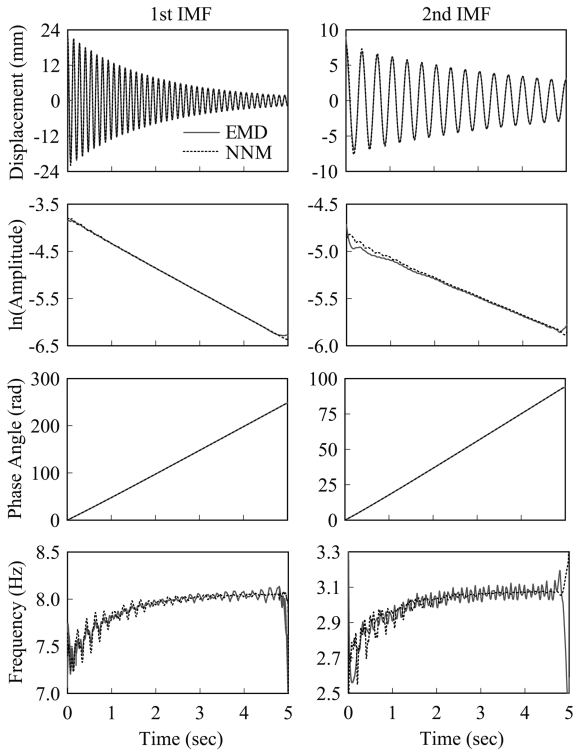

Fig. 13 Comparison of the results obtained from the IMF components of the displacement response and the NNM method for Case 3 (1st story)

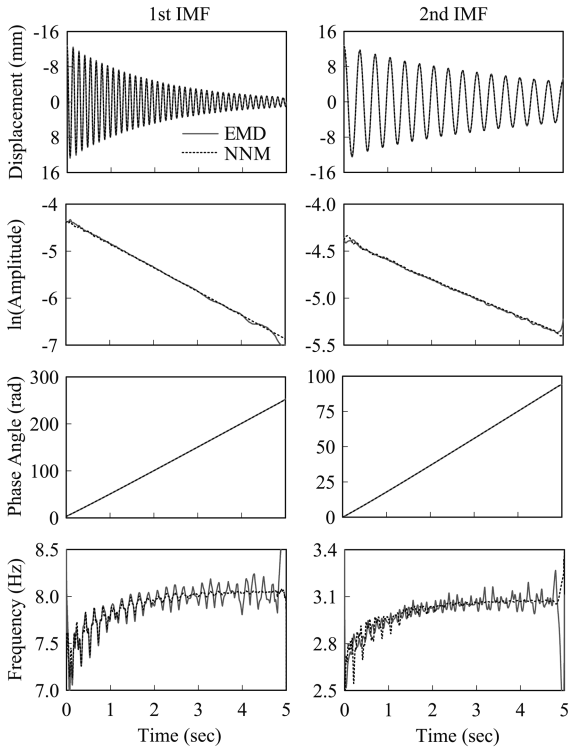

Fig. 14 Comparison of the results obtained from the IMF components of the displacement response and the NNM method for Case 3 (2nd story)

for this nonlinear case. The responses from the RK method were then processed through the EMD to produce IMF components. Fig. 13 shows the comparison of the IMF components and the NNM responses together with their amplitudes and phase angles for the st story displacement responses. It is seen that all three quantities compare quite well. After the Hilbert transform, the instantaneous frequencies from the IMF components and the NNM responses were obtained and plotted at the bottom of Fig. 13. The results show that the instantaneous frequencies of the 1st and the 2nd IMF exhibit an increasing trend from about 7.5 Hz to 8.0 Hz and about 2.7 Hz to 3.1 Hz, respectively, as their response amplitudes reduce. The IMF and the NNM frequencies match well in terms of their mean trends though exhibit differences in their local fluctuations. Comparisons for the 2nd story are shown in Fig. 14 and similar results are observed. The two instantaneous mode shapes can be obtained by comparing the corresponding IMF components of the displacement responses at the two stories as shown in Fig. 15. The results once again confirm that the two instantaneous mode shape ratios obtained from the IMF components are very close to the respective analytical linear mode shape values. Hence the nonlinear state matrix **D** can be obtained from Eq. (15) through the sequential quadratic programming algorithm. The identified parameters for this case are also summarized in Table 1. It is seen the errors for the linear stiffness coefficients are less than 2% and that for the damping coefficients are less then 4%. As for the nonlinear stiffness coefficients, it is seen that k_{1r} and k_{2r} are identified with 8% and 14% error, respectively.

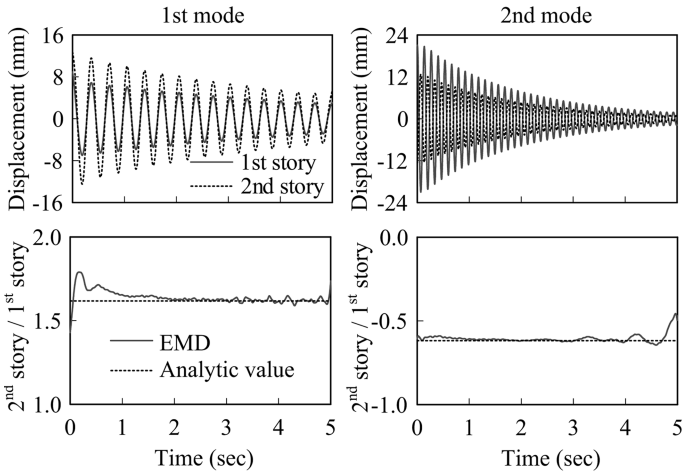

Fig. 15 IMF components obtained from the displacement responses of two stories and their amplitude ratios for Case 3

6. Conclusions

The EMD method is well-known for its ability to decompose a multi-component signal into a set of IMFs. The method uses a sifting process in which local time-scale extrema of a signal are used together with a spline fitting approximation for decomposition. This method provides an effective and robust approach for decomposing nonlinear and non-stationary signals. On the other hand, the IMF components do not automatically guarantee a well-defined physical meaning hence it is necessary to validate the IMF components carefully prior to any further processing and interpretation. In this paper, an attempt to use the EMD method for identifying properties of nonlinear elastic MDOF structures was explored. It was first shown that the IMF components of the displacement and velocity responses of a nonlinear elastic structure were numerically close to the NNM responses obtained from two-dimensional invariant manifolds. The IMF components could then be used in the context of the NNM method to estimate the properties of the nonlinear elastic structure. A two-degree-of-freedom shear-beam building model was used as an example to illustrate the proposed technique. Three different levels of nonlinearity were assumed: linear model, nonlinearity occurs between the ground and the 1st story, and nonlinearity occurs at both stories. Numerical results showed that the combined EMD and NNM method was able to estimate the properties of the nonlinear elastic model reasonably well. The estimation errors were mainly attributed from the residual errors associated with the sifting process in the EMD method. The effect of measurement noise was also studied in this paper using two noise removal techniques: the Fourier-based band-pass filtering technique and the wavelet-based denoising technique. The noise-polluted responses were processed through the noise removal techniques prior to using the EMD method. Results showed that the linear parameters of the building model could still be accurately estimated for both noise removal techniques. The Fourier-based band-pass filtering technique however failed to identify the nonlinear parameters as it removed the intrawave harmonic components that were needed for modeling the nonlinear characteristics in the responses. The wavelet-based denoising technique on the other hand appeared to be less affected by the presence of measurement noise and still could estimate the nonlinear parameters fairly well. Although the numerical results were obtained using

a building model with only two degrees of freedom, the proposed technique can be used to identify nonlinear properties of structures with a larger number of degrees of freedom. It however should be noted that the increase of degrees of freedom not only requires more computational effort but also leads to potential numerical difficulties associated with convergence of the constrained nonlinear optimization algorithm. From the computational viewpoint, it might be beneficial to use the proposed technique together with a nonlinear order reduction algorithm to minimize computational effort and alleviate possible numerical difficulty.

Acknowledgement

This study is supported by the Hong Kong Research Grants Council Competitive Earmarked Research Grant 611405.

References

Donoho, D. L. (1995), "De-noising by soft-thresholding", *IEEE Transactions on Information Theory*, **41**(3), 613-627.

Farrar, C. R., Doebling, S. W. and Nix, D. A. (2001), "Vibration-based structural damage identification", *Philosophical Transactions of the Royal Society of London Series A-Mathematical Physical and Engineering Sciences*, **359**, 131-149.

Feldman, M. (1994a), "Non-linear system vibration analysis using Hilbert transform-I. Free vibration analysis method 'FREEVIB' ", *Mechanical Systems and Signal Processing*, **8**(2), 119-127.

Feldman, M. (1994b), "Non-linear system vibration analysis using Hilbert transform-II. Forced vibration analysis method 'FORCEVIB' ", *Mechanical Systems and Signal Processing*, **8**(3), 309-318.

Gurley, K. and Kareem, A. (1999), "Application of wavelet transform in earthquake, wind and ocean engineering", *Eng. Struct.*, **21**, 149-167.

Hahn, S. L. (1996), *Hilbert Transforms in Signal Processing*, Boston : Artech House, 442pp.

Huang, N. E., Shen, Z., Long, S. R., Wu, M. C., Shih, H. H., Zheng, Q., Yen, N.-C., Tung, C. C. and Liu, H. (1998a), "The empirical mode decomposition and the Hilbert spectrum for nonlinear and non-stationary time series analysis", *Proceedings of the Royal Society of London, Series A*, **454**, 903-995.

Huang, N. E., Shen, Z. and Long, S. R. (1998b), "A new view of nonlinear water waves: the Hilbert spectrum", *Annual Review of Fluid Mechanics*, **31**, 417-457.

Rilling, G., Flandrin, P. and Goncalves, P. (2003), "On empirical mode decomposition and its algorithms", *IEEE-EURASIP Workshop on Nonlinear Signal and Image Processing NSIP-03*. Shaw S. W. and Pierre C. (1993). "Normal modes for non-linear vibratory systems", *J. Sound Vib.*, **164**(1), 85-124.

Schittowski, K. "NLQPL: A FORTRAN-subroutine solving constrained nonlinear programming problems", *Annuals of Operations Research*, **5**, 485-500.

Yang, J. N., Lei, Y., Pan, S. and Huang, N. (2003a), "Identification of linear structures based on Hilbert-Huang transform. Part 1: normal modes", *Earthq. Eng. Struct. Dyn.*, **32**(9), 1443-1467.

Yang, J. N., Lei, Y., Pan, S. and Huang, N. (2003b), "Identification of linear structures based on Hilbert-Huang transform. Part 2: complex modes", *Earthq. Eng. Struct. Dyn.*, **32**(10), 1533-1554.

Zhao, J. and DeWolf, J. T. (1999), "Sensitivity study for vibrational parameters used in damage detection", *J. Struct. Eng.*, ASCE, **125**(4), 410-416.

CC